SUPPLEMENTARY INFORMATION

Silicon Redistribution, Acid Site Loss and the Formation of a Core-Shell Texture upon Steaming SAPO-34 and their Impact on Catalytic Performance in the MTO Reaction.

Ivalina B. Minova, Nathan S. Barrow, Andrea C. Sauerwein, Aaron B. Naden, David B. Cordes, Alexandra M. Z. Slawin, Stephen Schuyten and Paul A. Wright

---

Table of Content:

S1. Results Part I

Selected polished samples were measured on a Hitachi S-4800 SEM instrument (Figure S1), with the electron beam at 5 kV for SEM and 15 kV for EDX measurements (sample was coated with carbon <20 nm layer prior to analysis).

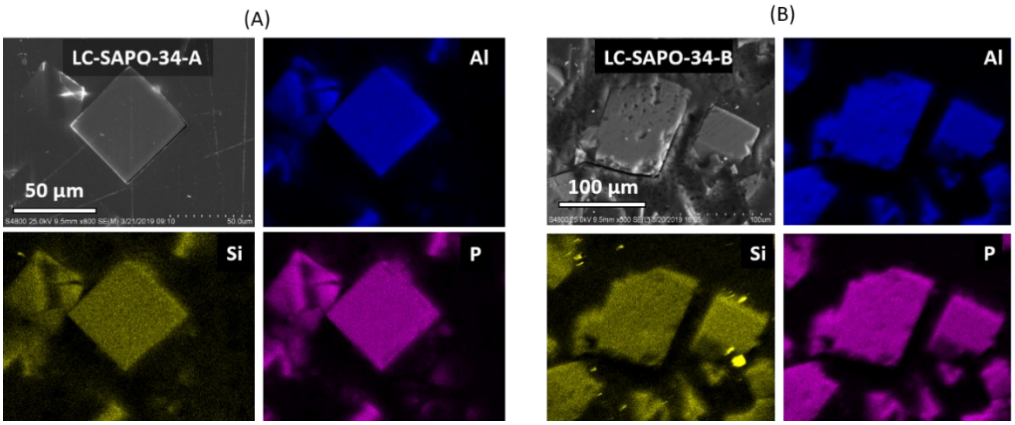

Figure S1. Elemental distribution derived from EDX map across a cross section of polished (A) LC-SAPO-34-A and (B) LC-SAPO-34-B.

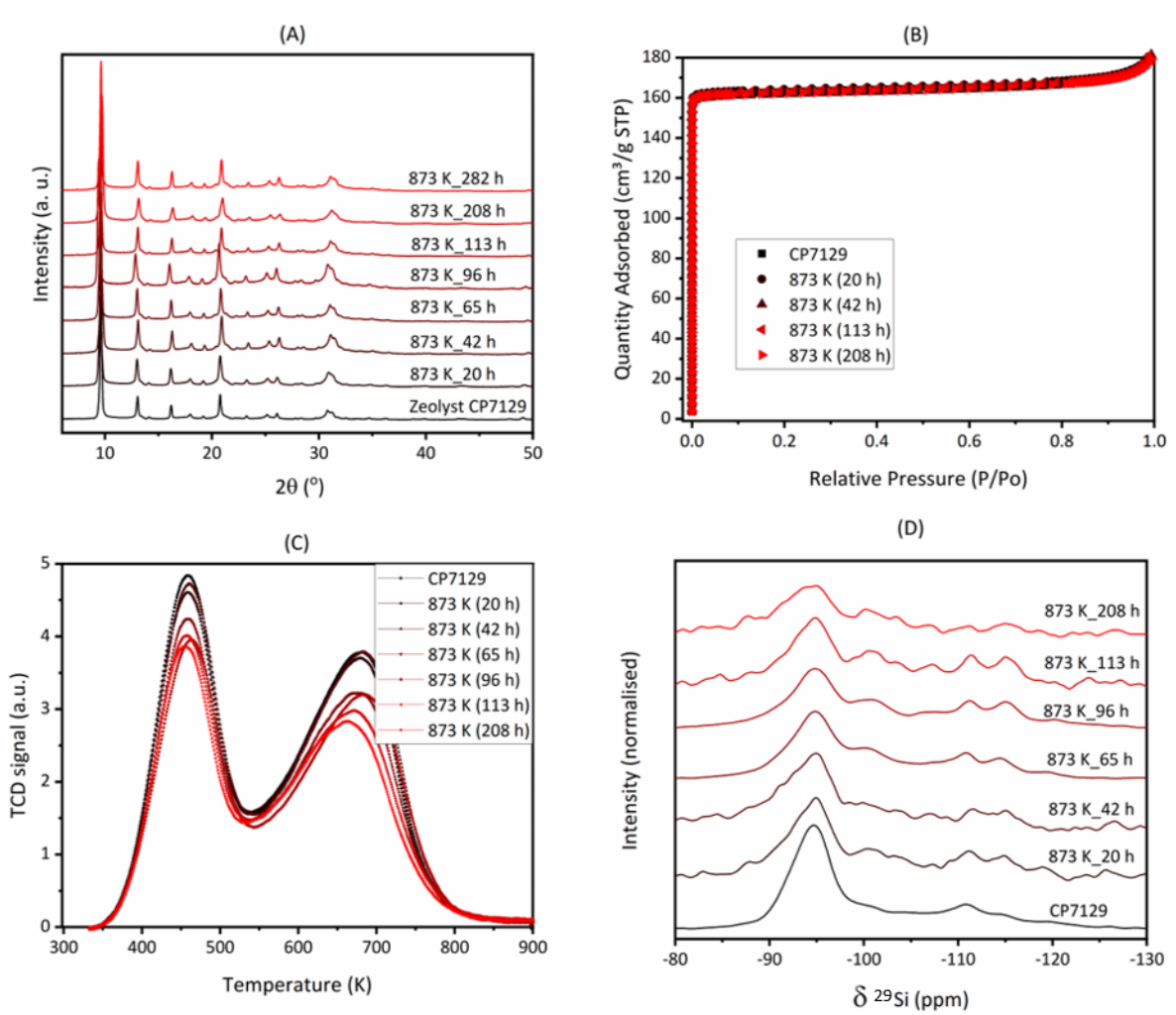

Figure S2. Zeolyst CP7129 HSAPO-34 steamed at 873 K between 20 h and 208 h. (A) PXRD patterns; (B) N_2 isotherms (77 K); (C) NH_3-TPD profiles normalised against mass and (D) ^{29}Si MAS ssNMR spectra normalized by mass and number of scans.

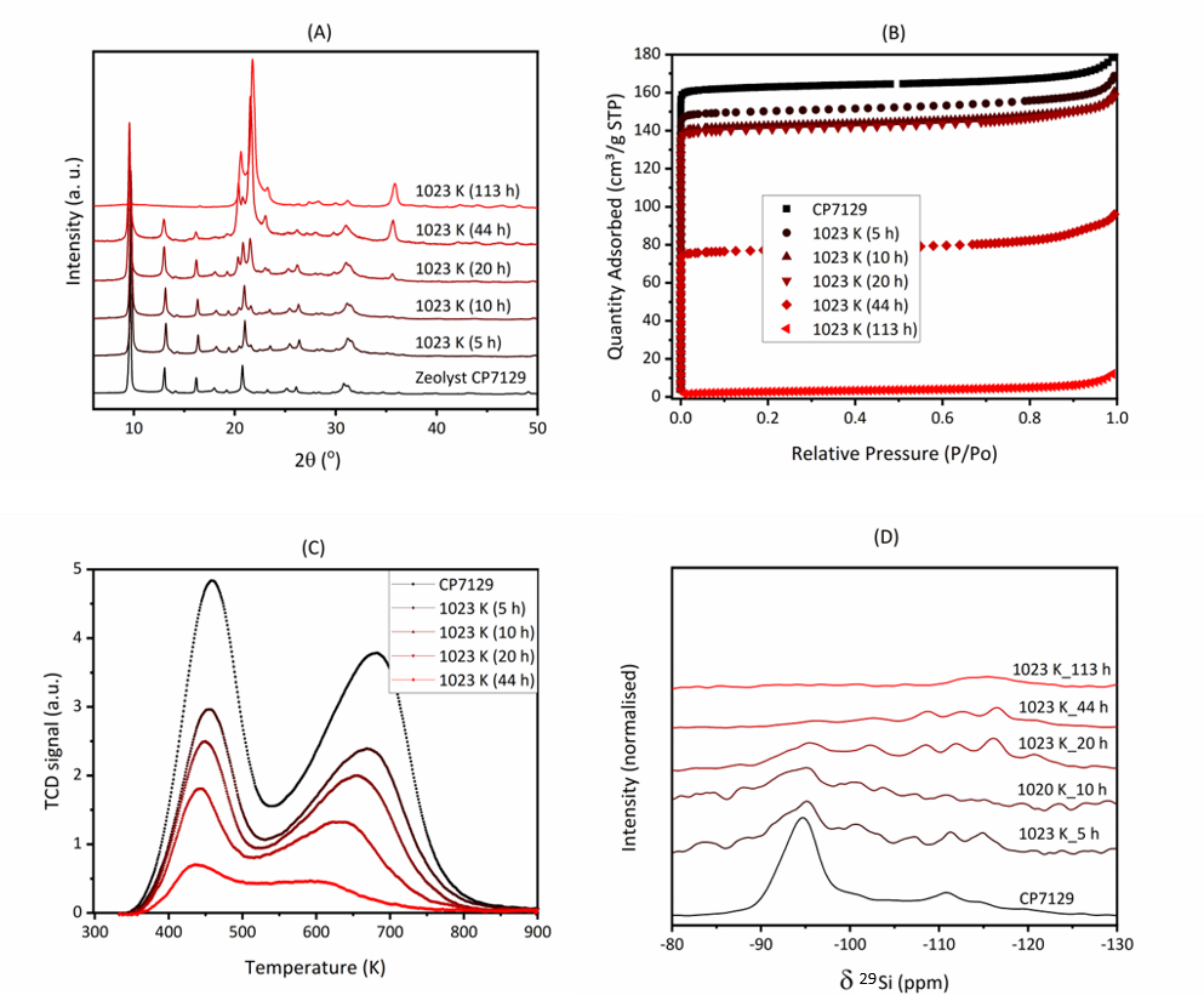

Figure S3. CP7129 HSAPO-34 steamed at 1023 K between 20 h and 113 h. (A) PXRD patterns; (B) N_2 isotherms (77 K); (C) NH_3-TPD profiles normalised against mass and (D) ^{29}Si MAS ssNMR spectra normalized by mass and number of scans.

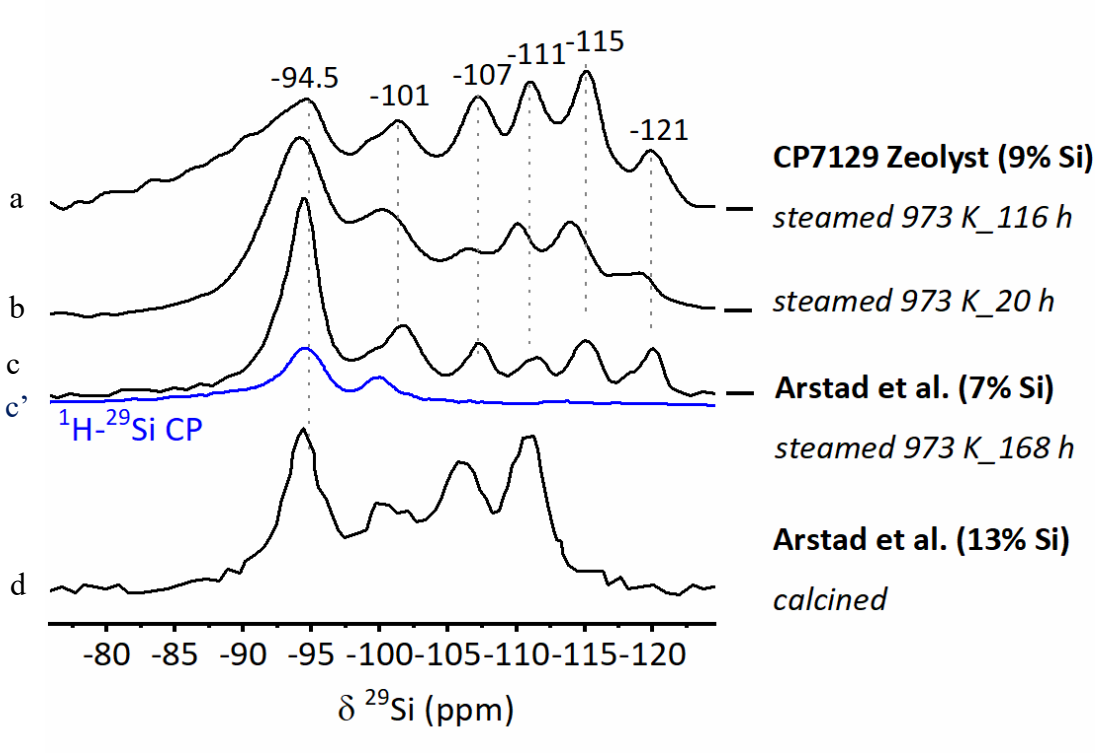

Figure S4. Directly acquired ^{29}Si MAS ssNMR spectra (black) of (a) CP7129-973-116 and (b) CP7129-973-20 compared with SAPO-34 spectra reported by Arstad et al[1]: (c) steamed 7% SAPO-34, (c') in blue ^{1}H--^{29}Si cross-polarization spectrum of steamed 7% SAPO-34, and (d) high, 13% Si, non-steamed- SAPO-34. Literature spectra were digitized on Origin Pro.

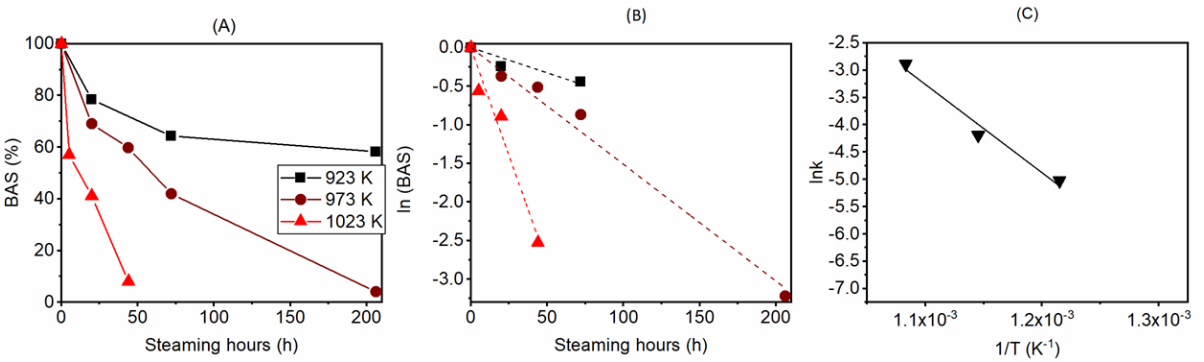

Figure S5. (A) BAS expressed as a % relative to the calcined (non-steamed) LC-SAPO-34-A and (B) corresponding logarithmic plots, respectively. (C) lnk versus 1/T trendline and E_a values derived for LC-SAPO-34-A.

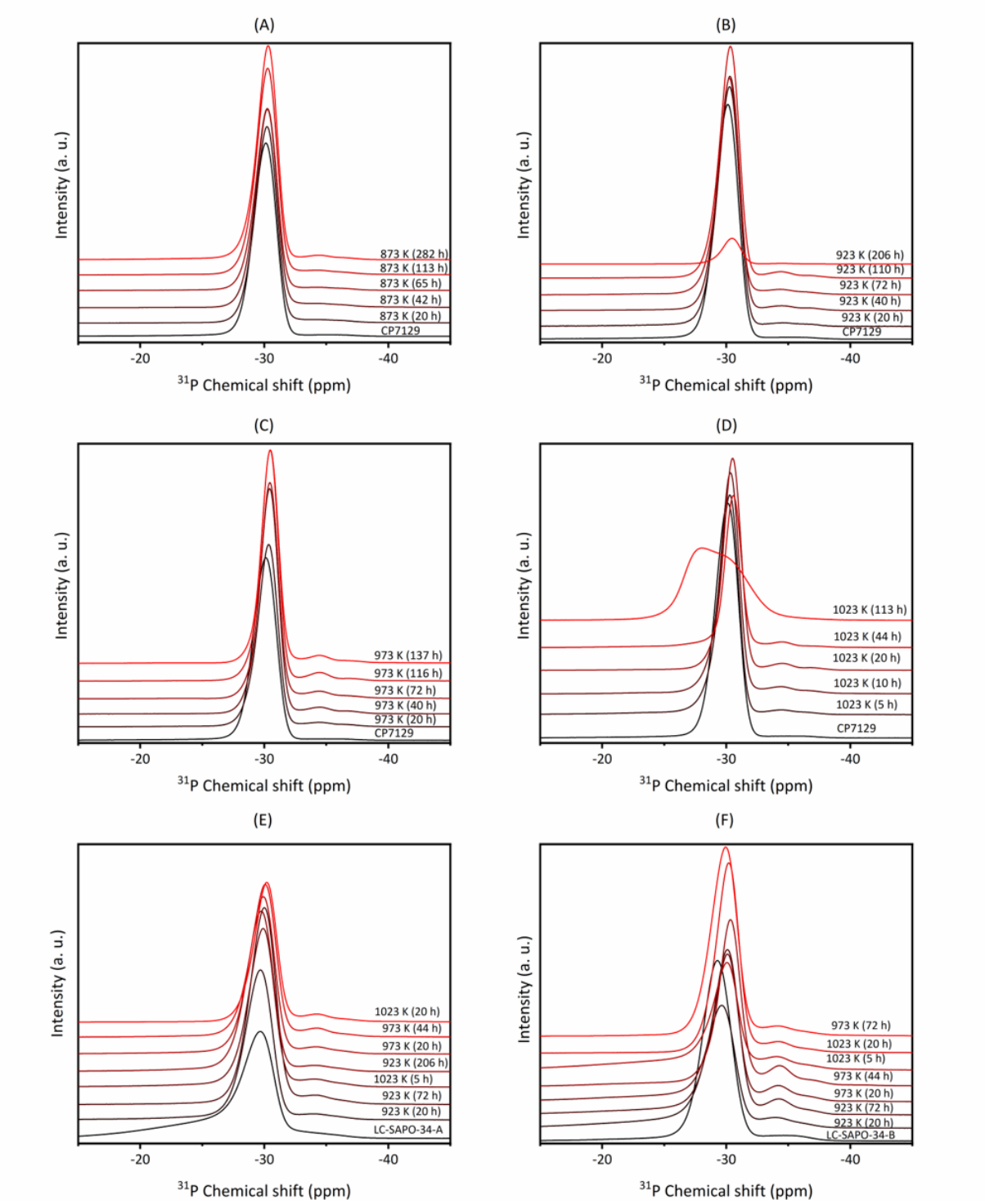

Figure S6. ^{31}P ssNMR spectra of (A-D) CP7129, (E) LC-SAPO-34-A and (F) LC-SAPO-34-B for the calcined and steamed samples at 873 K and higher temperatures, also different duration of steaming at each temperature

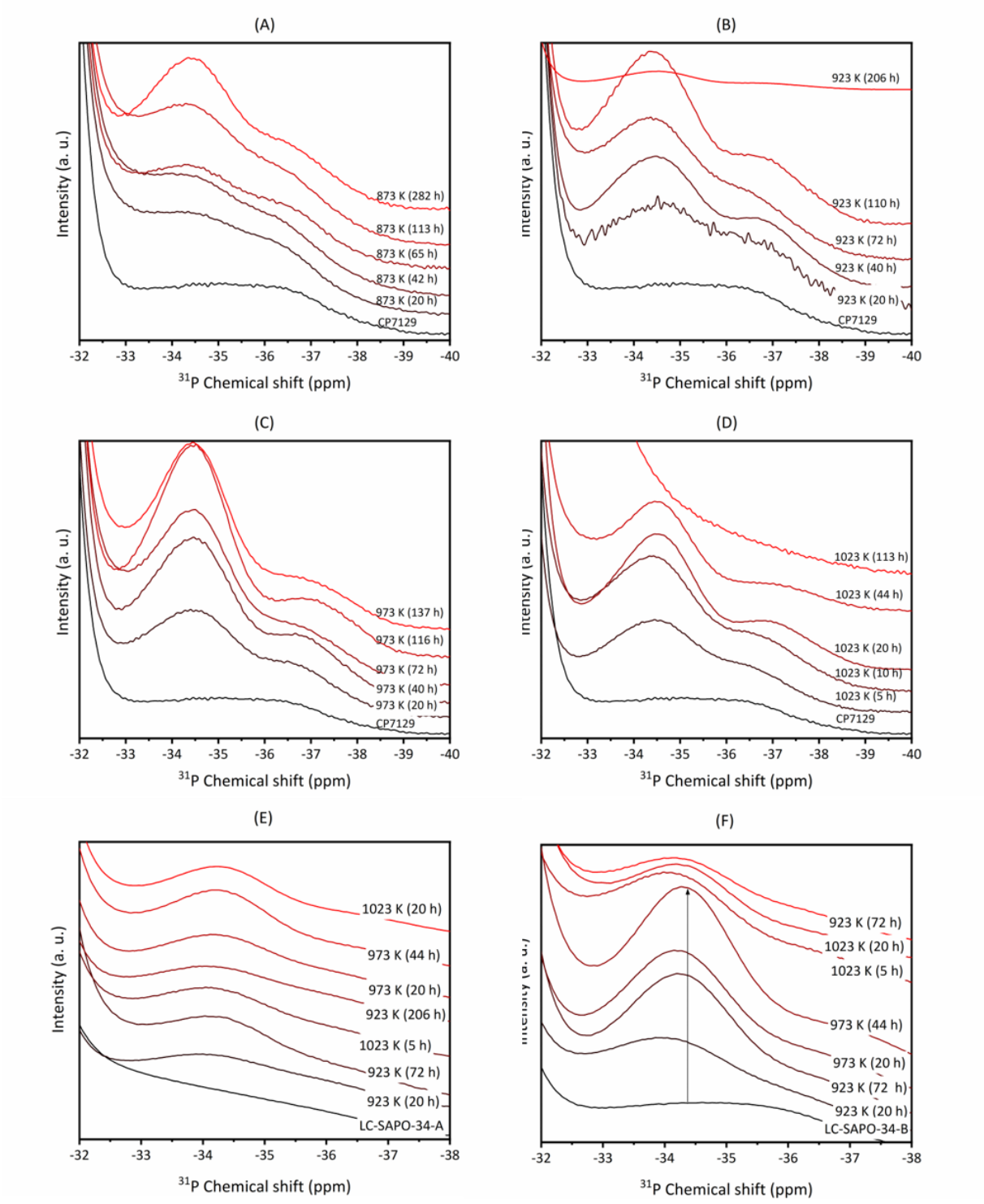

Figure S7. Expansion of the ^{31}P MAS ssNMR spectra; focus on the -34.4 ppm peak.

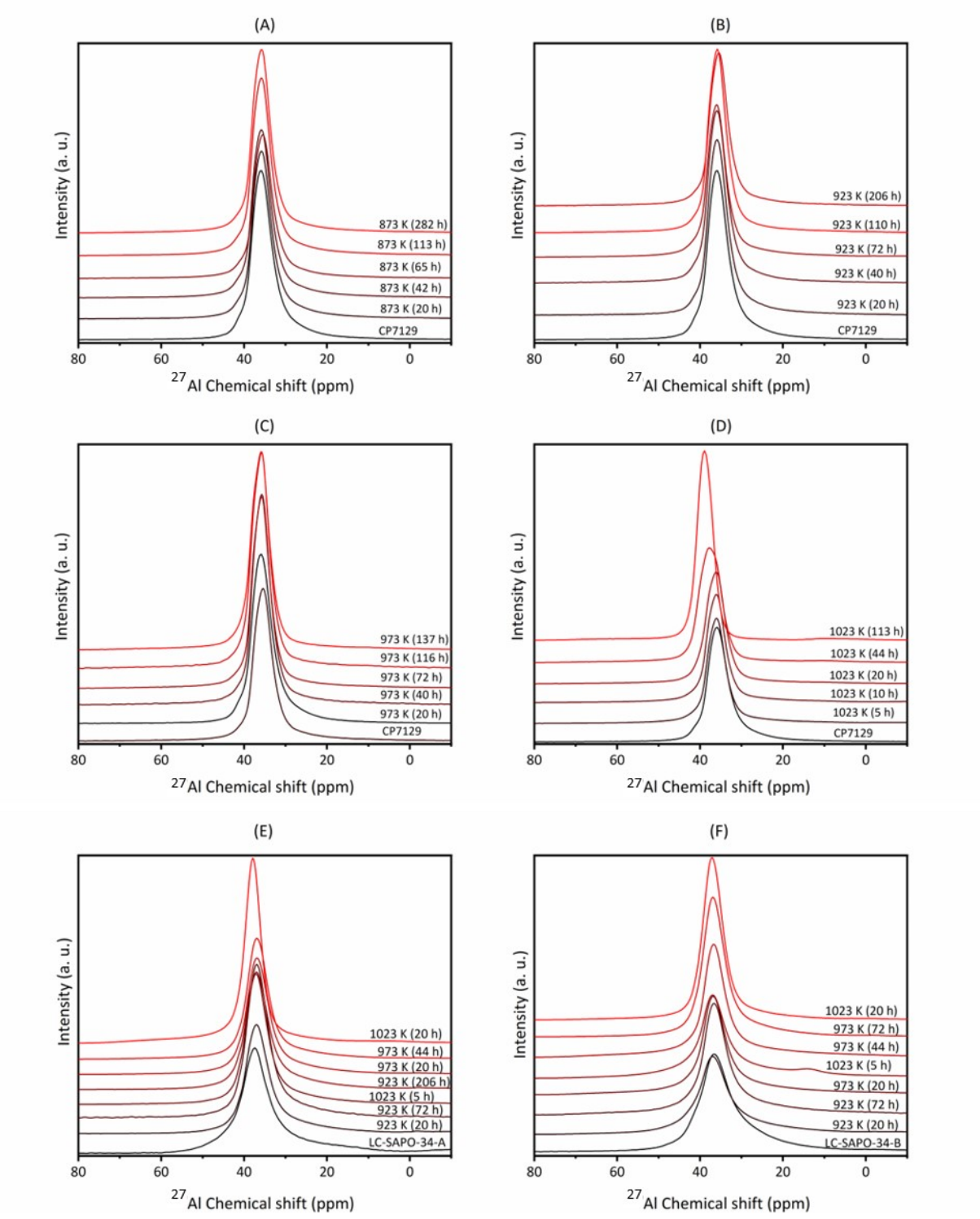

Figure S8. ^{27}Al MAS ssNMR spectra of (A-D) CP7129, (E) LC-SAPO-34-A and (F) LC-SAPO-34-B for the calcined and steamed samples at 873 K and higher temperatures, also different duration of steaming at each temperature

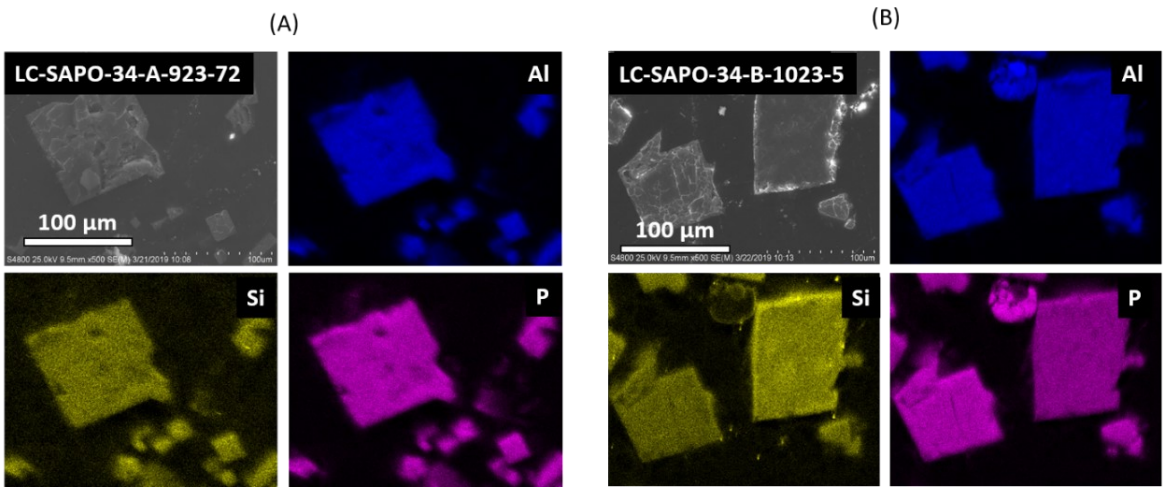

Figure S9. Elemental distribution derived from EDX map across the cross section of polished (A) LC-SAPO-34-A steamed at 923 K for 72 h and (B) LC-SAPO-34-B steamed at 1023 K for 5 h.

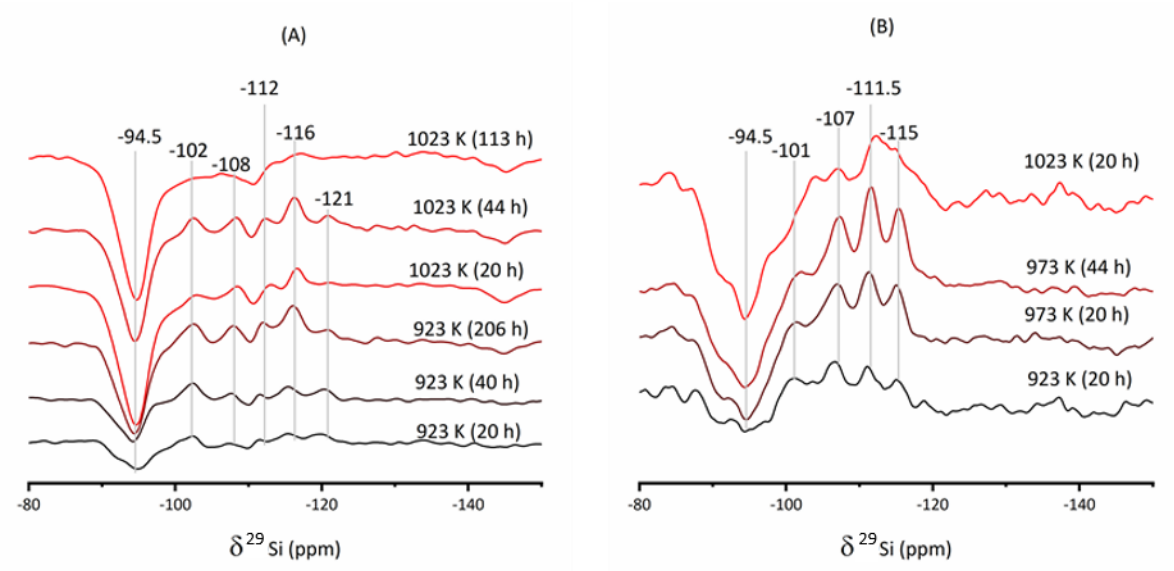

Figure S10. Difference ^{29}Si MAS ssNMR on (A) CP7129 and (B) LC-SAPO-34-B highlighting the growth of new ^{29}Si resonances with progressive steaming. The spectrum of the calcined material in each sample was used for the subtraction.

Histogram of pore sizes was evaluated from the cross-sectional SEM images after thresholding the image using the ImageJ software; the minimum size used for pore identification was set to 0.001 μm^2 to remove any pixel-to-pixel noise.

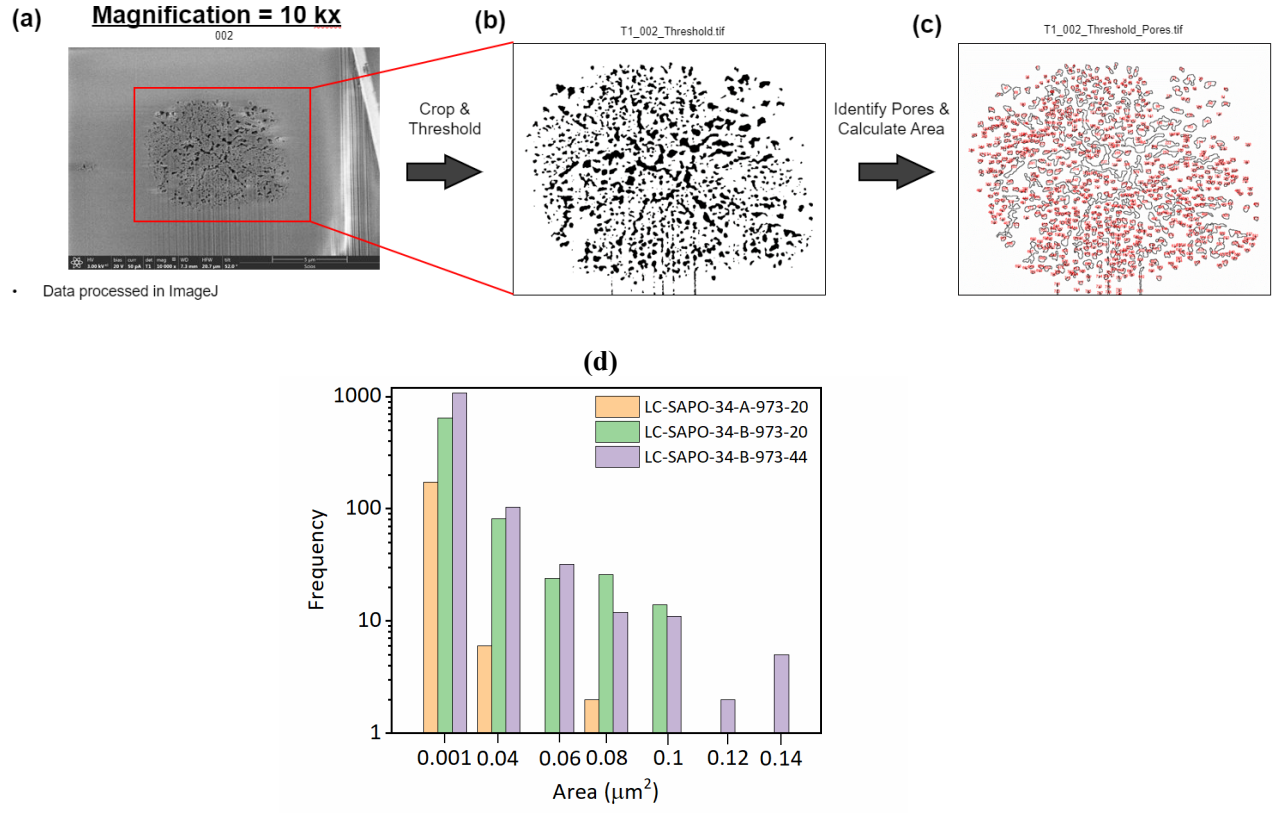

Figure S11. (a) Example cross-sectional FIB-SEM image of steamed SAPO-34, (b) image after thresholding and (c) annotated image after pore identification; (d) Histogram of pore size distribution in the 10^{-3} to 10^{-1} μm^2 range of large crystals of LC-SAPO-34-A-973-20, LC-SAPO-34-B-973-20 and LC-SAPO-34-B-973-44.

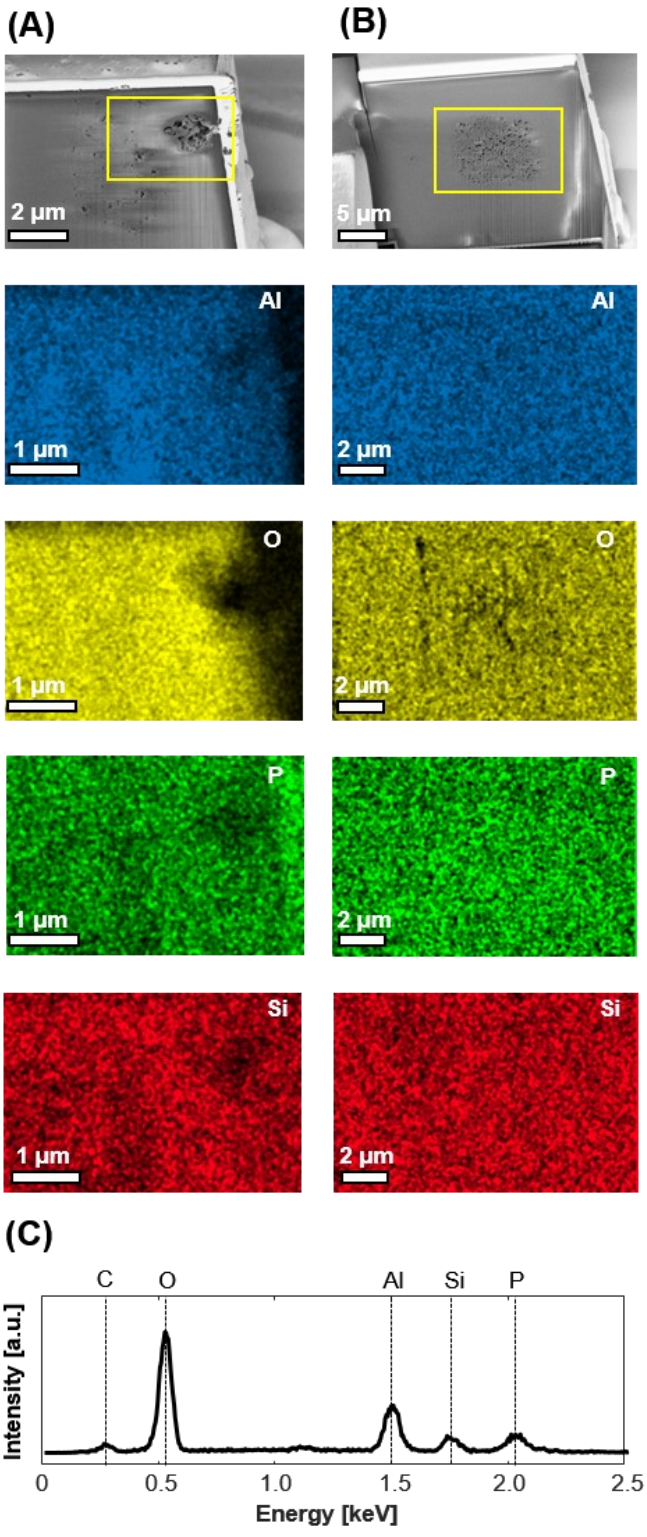

Figure S12. Cross-sectional FIB-SEM-EDX map of the elemental composition in (A) LC-SAPO-34-A-973-20 and (B) LC-SAPO-34-B-973-20 showing a uniform distribution of the elements in both samples; (C) representative EDX spectrum (5 kV) for sample A.

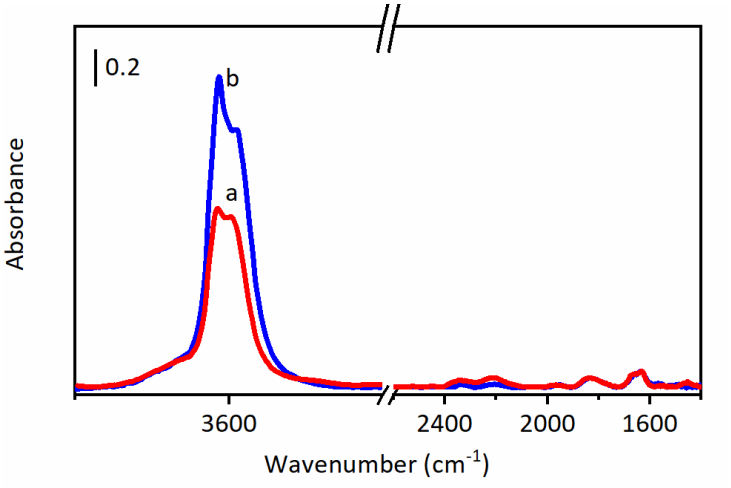

Figure S13. Representative synchrotron FTIR spectra of individual crystals collected in transmission for calcined single crystals of sample (a) LC-SAPO-34-A and (b) LC-SAPO-34-B, both dehydrated at 623 K in nitrogen.

Table S1. Selected crystallographic data (SCXRD analysis).

Dehydrated samples	**LC-SAPO-34-B**	**Steamed LC-SAPO-34-B-973-44**
empirical formula	$Al_{18}O_{72}P_{14}Si_4$	$Al_{18}O_{72}P_{14}Si_4$
formula weight	2183.58	2183.58
crystal description	colourless prism	colourless prism
crystal size [mm^3]	0.09×0.09×0.04	0.08×0.07×0.03
space group	$R\bar{3}$	$R\bar{3}$
***a* [Å]**	13.5836(2)	13.5348(6)
***c* [Å]**	14.8221(4)	14.7549(12)
volume [Å]^3	2368.48(10)	2340.8(3)
Z	1	1
ρ (calculated) [g/cm^3]	1.531	1.549
μ [mm^{-1}]	5.414	5.478
F(000)	1076	1076
reflections collected	8354	8201
independent reflections (R_{int})	967 (0.0428)	959 (0.0496)
parameters, restraints	56, 0	56, 0
GOF on F^2	1.862	1.661
R_1 [$I > 2\sigma(I)$]	0.1031	0.1409
wR_2 (all data)	0.3729	0.4001
largest diff. peak/hole [e/Å^3]	0.84, -0.41	1.16, -0.51

Table S2. Bond distances and angles from SCXRD analysis of LC-SAPO-34-B.

Distance (Å) /Angle (°)	**LC-SAPO-34-B Calcined**	**LC-SAPO-34-B Steamed 973K 44h**
Al-O1	1.684(4)	1.646(6)
Al-O2	1.697(5)	1.656(7)
Al-O3	1.669(4)	1.635(6)
Al-O4	1.715(4)	1.699(6)
Mean Al–O	1.691	1.659
P(Si)-O1	1.531(4)	1.556(6)
P(Si)-O2	1.545(5)	1.536(7)
P(Si)-O3	1.537(4)	1.563(6)
P(Si)-O4	1.526(4)	1.534(6)
Mean P–O	1.535	1.547
O1-Al-O2	112.0(3)	112.7(4)
O1-Al-O4	108.4(3)	108.7(4)
O2-Al-O4	109.6(2)	107.6(4)
O3-Al-O1	108.4(3)	110.3(4)
O3-Al-O2	108.4(3)	108.6(4)
O3-Al-O4	110.0(2)	108.7(4)
O1-P-O2	112.0(3)	113.3(4)
O1-P-O3	107.2(3)	106.7(4)
O3-P-O2	108.2(3)	107.6(4)
O4-P-O1	108.1(3)	107.9(4)
O4-P-O2	110.3(3)	108.7(4)
O4-P-O3	111.0(3)	112.8(4)

Table S3. Refinement parameters for dehydrated SAPO-34 calcined and steamed samples CP7129 and LC-SAPO-34-B analysed by Rietveld refinement.

Dehydrated samples	**CP7129**	**Steamed CP7129-973-20**	**LC-SAPO-34-B**	**Steamed LC-SAPO-34-B-973-44**
Composition	$AlP_{0.8}Si_{0.2}O_4$	$AlP_{0.8}Si_{0.2}O_4$	$AlP_{0.8}Si_{0.2}O_4$	$AlP_{0.8}Si_{0.2}O_4$
Diffractometer	Stoe STADI P	Stoe STADI P	Stoe STADI P	Stoe STADI P
Wavelength / Å	1.54056	1.54056	1.54056	1.54056
Range / º2θ	7 - 65	6 - 65	6 - 65	7 - 65
Space Group	*R* –3	*R* –3	*R* –3	*R* –3
Z	18	18	18	18
R_{wp}; R_p /%	11.0; 8.4	10.1; 7.7	8.8; 5.7	8.9; 6.5
***a* / Å**	13.7429(10)	13.7194(14)	13.7382(9)	13.6756(8)
***c* / Å**	14.9766(20)	14.9545(29)	14.9748(24)	14.8638(15)
V / Å^3	2449.6(5)	2437.6(7)	2447.6(5)	2407.4(4)

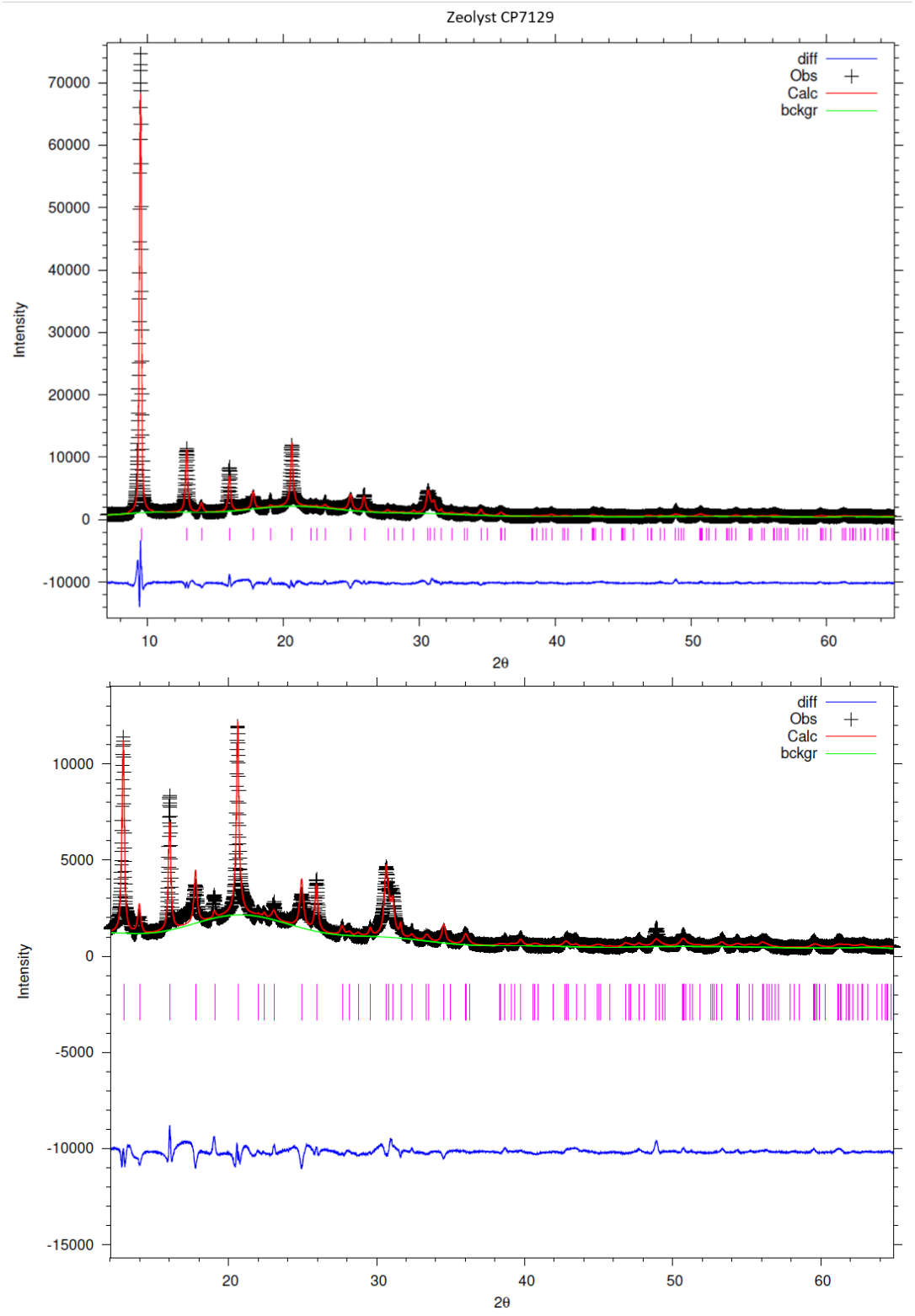

Figure S14. Rietveld plot for calcined, dehydrated Zeolyst (CP7129) SAPO-34. Data were collected at room temperature (RT) (λ=1.5406 Å) and are depicted as follows: observed data (crosses), calculated profile (purple line), difference (blue line). Tick marks indicate the predicted peak positions from the unit cell.

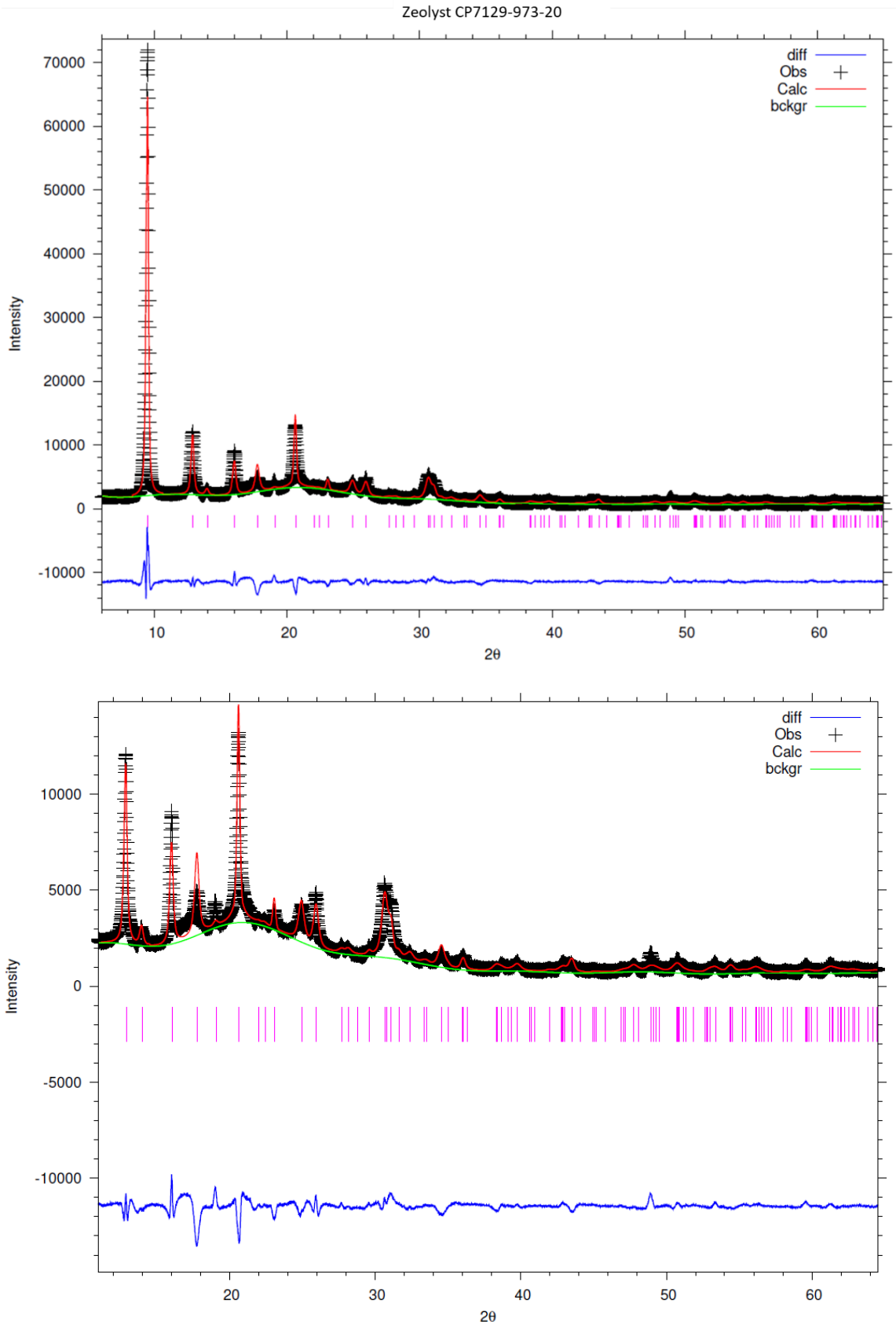

Figure S15. Rietveld plot for CP7129-973-20 steamed, dehydrated, with expansion.

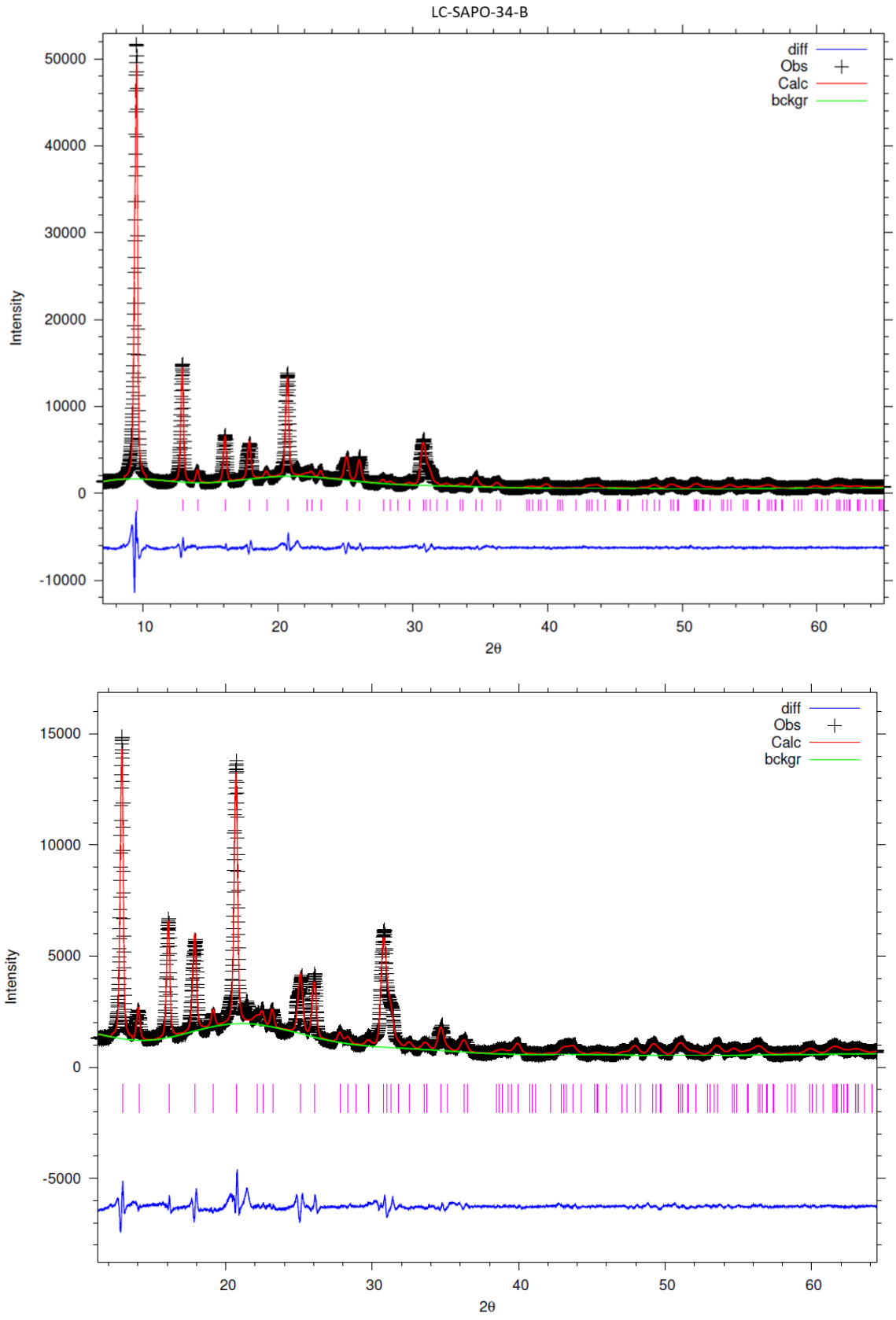

Figure S16. Rietveld plot for LC-SAPO-34-B calcined, dehydrated, with expansion.

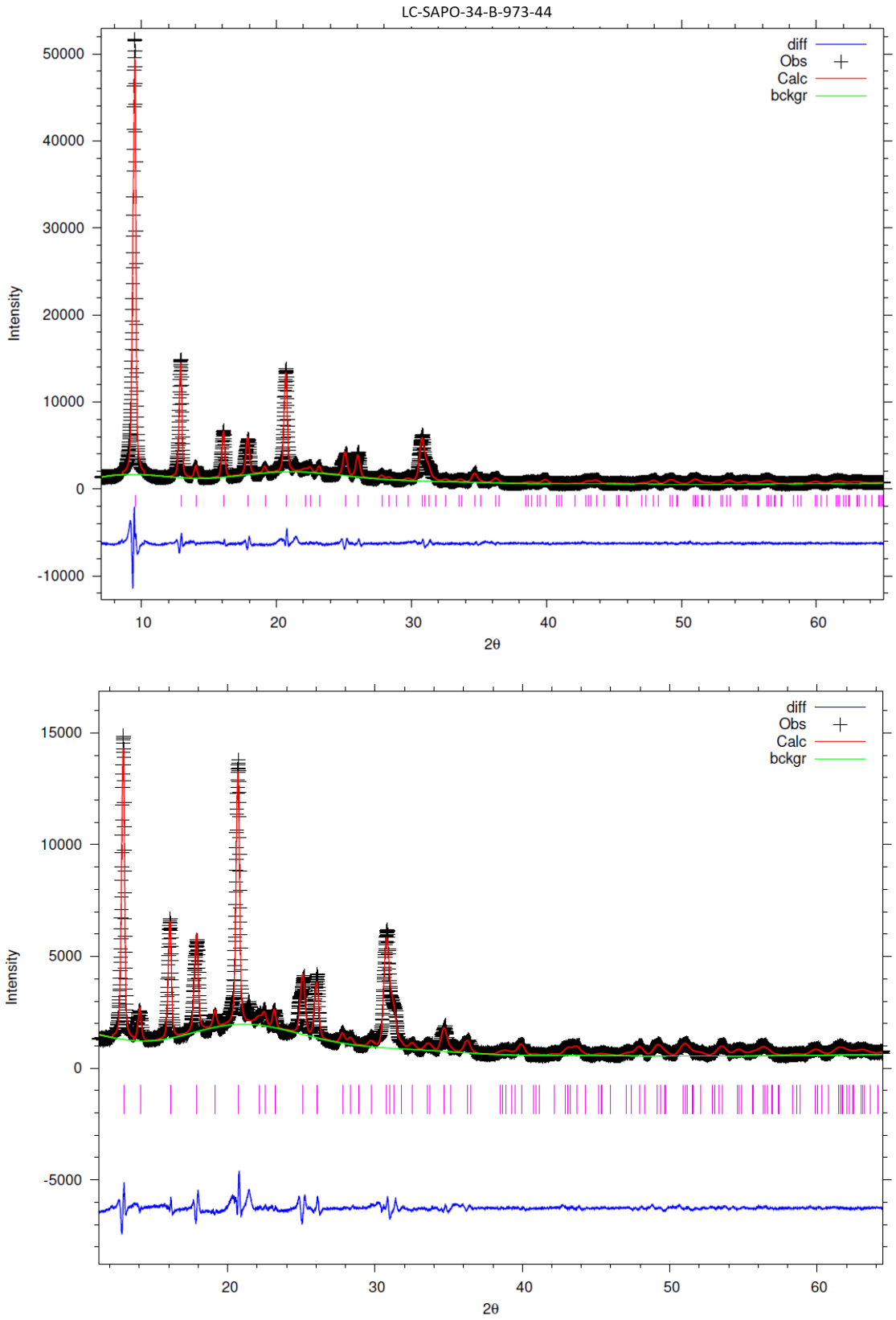

Figure S17. Rietveld plot for LC-SAPO-34-B-973-44 steamed, dehydrated, with expansion.

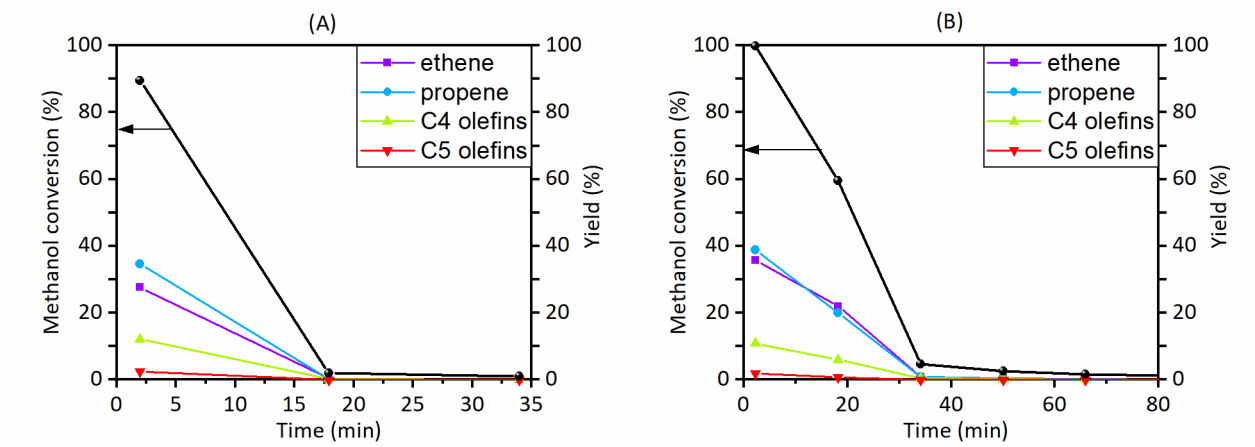

Figure S18. Effluent stream alkane and olefin yields percentage for the methanol-to-olefins reaction over calcined LC-SAPO-34-A at 723 K; the black line represents the methanol conversion. Testing conditions: (A) 95% CH_3OH in water, WHSV(CH_3OH) = 7 h^{-1} and (B) 40% CH_3OH in water, WHSV(CH_3OH) = 3 h^{-1}.

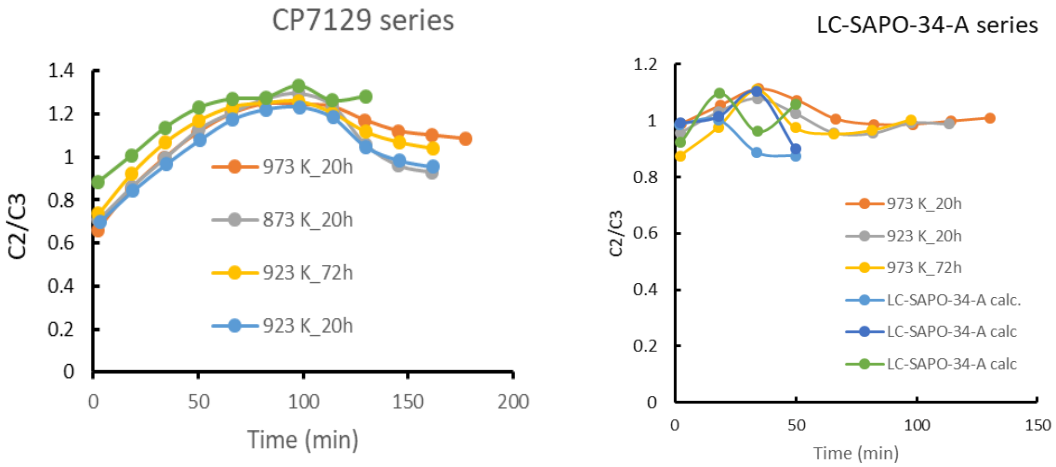

Figure S19. Molar ethylene/propylene (C2/C3) ratios in light olefin products from MTO reaction over (left) CP7129 SAPO-34 (WHSV(CH_3OH) = 7 h^{-1} and (right) LC-SAPO-34-A SAPO-34 (WHSV(CH_3OH) = 3 h^{-1}) steamed under different, specified, conditions.

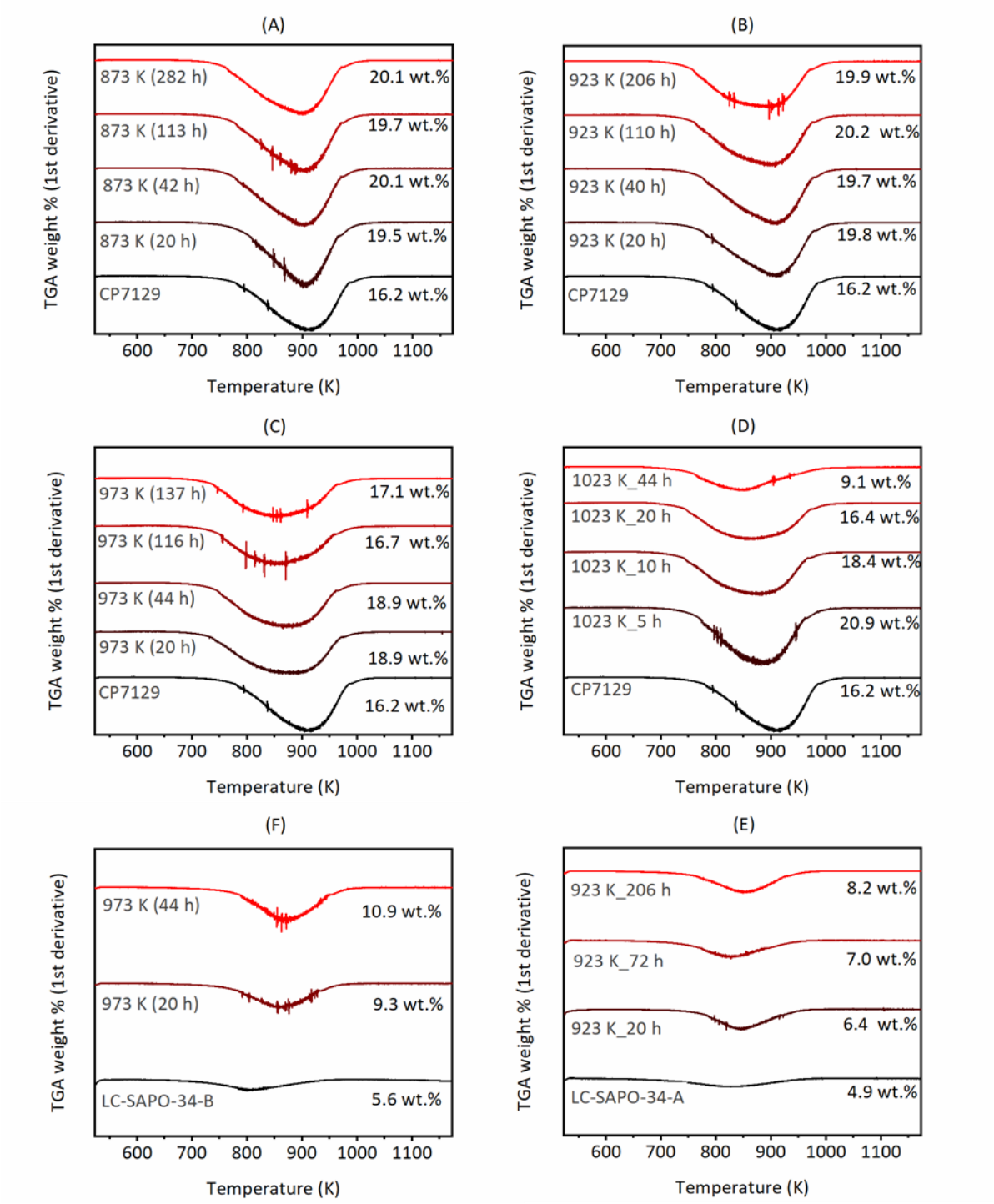

Figure S20. DTGA profiles for (A-D) CP7129, (E) LC-SAPO-34-A and (F) LC-SAPO-34-B changes with progressive steaming at different steaming durations and steaming temperatures. Values report the total wt.% of coke measured by TGA.

S2. Results Part II (SR-IR)

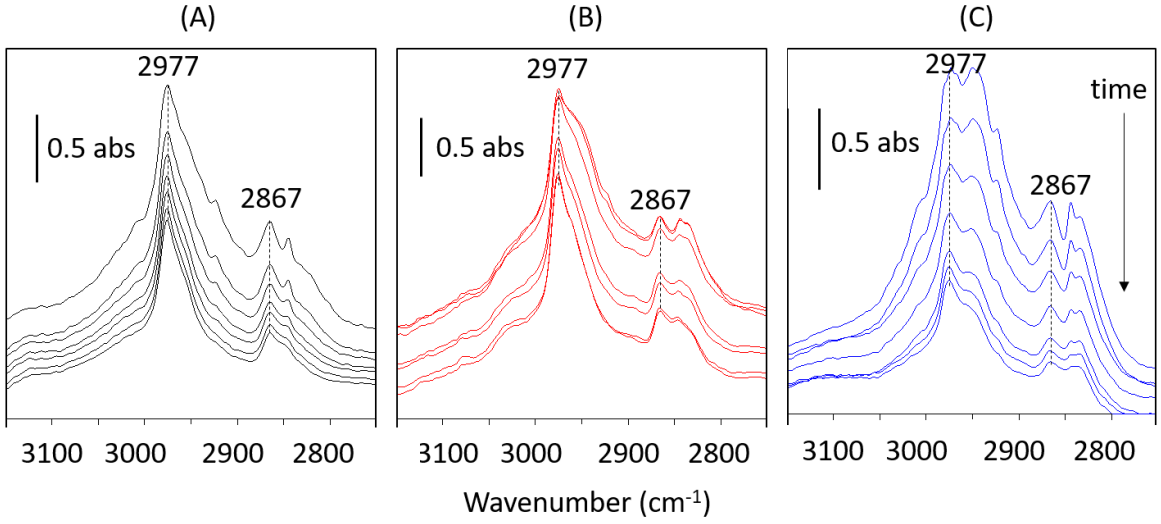

Figure S21. SR-IR difference spectra in the ν(CH) region at 20 s intervals between 80 and 200 s showing the loss of adsorbed DME during the trailing edge of an 8 μL pulse of CH_3OH at 573 K on (A) LC-SAPO-34-A (black), (B) LC-SAPO-34-A steamed at 973 K for 20 h (red) and (C) LC-SAPO-34-B steamed at 973 K for 44 h (blue).

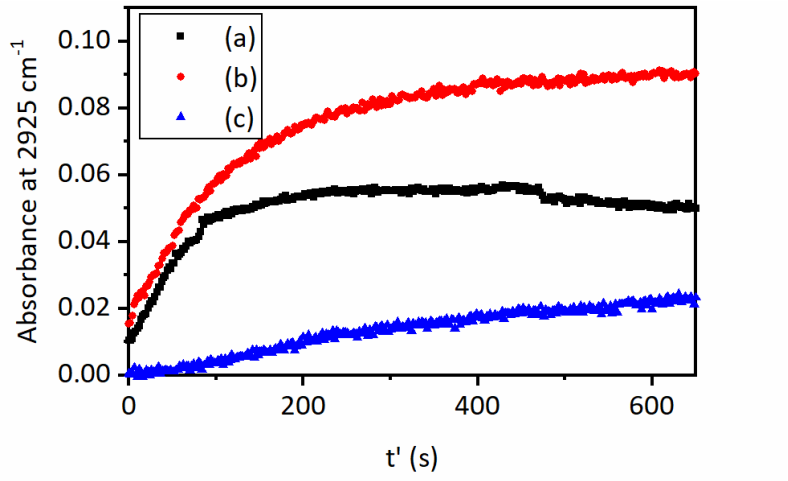

Figure S22. Time-course of the 2925 cm^{-1} intensity following 8 μL pulse of CH_3OH at 573 K on LC-SAPO-34-A (black), LC-SAPO-34-A steamed at 973 K for 20 h (red) and LC-SAPO-34-B steamed at 973 K for 44 h (blue).

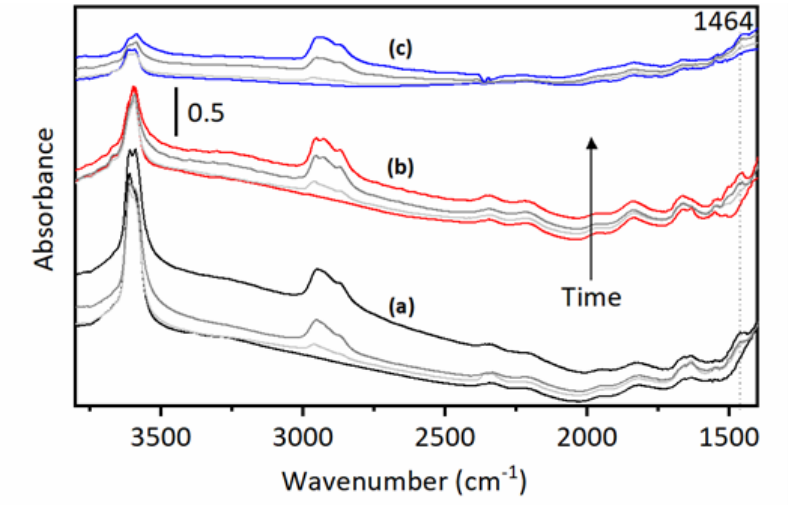

Figure S2319. SR-IR spectra at the end of each CH_3OH pulse (three pulses in total at 573 K) in (a) LC-SAPO-34-A and steamed (b) LC-SAPO-34-A-973-20 and (c) LC-SAPO-34-B-973-44.

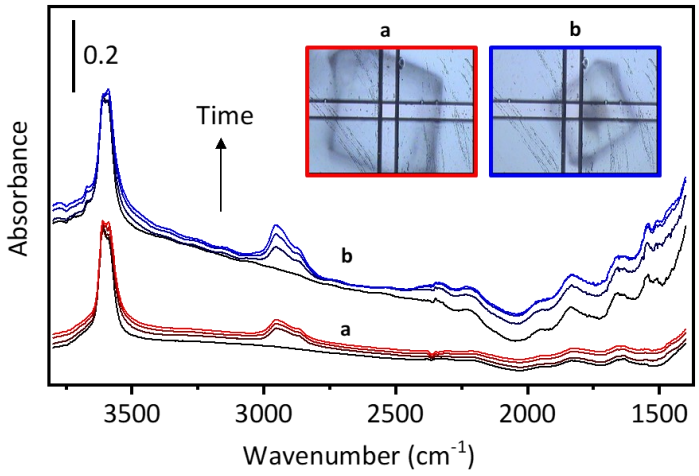

Figure S24. SR-IR spectra of (a) LC-SAPO-34-B fresh and (b) LC-SAPO-34-B-973-44 (the original absorbance intensity was scaled by a factor of 5× for clarity) steamed during exposure of 1, 2 and 3 pulses of CH_3OH at 623 K. Growth of organic species adsorbed with each pulse are more notable on the edge of the steamed sample.

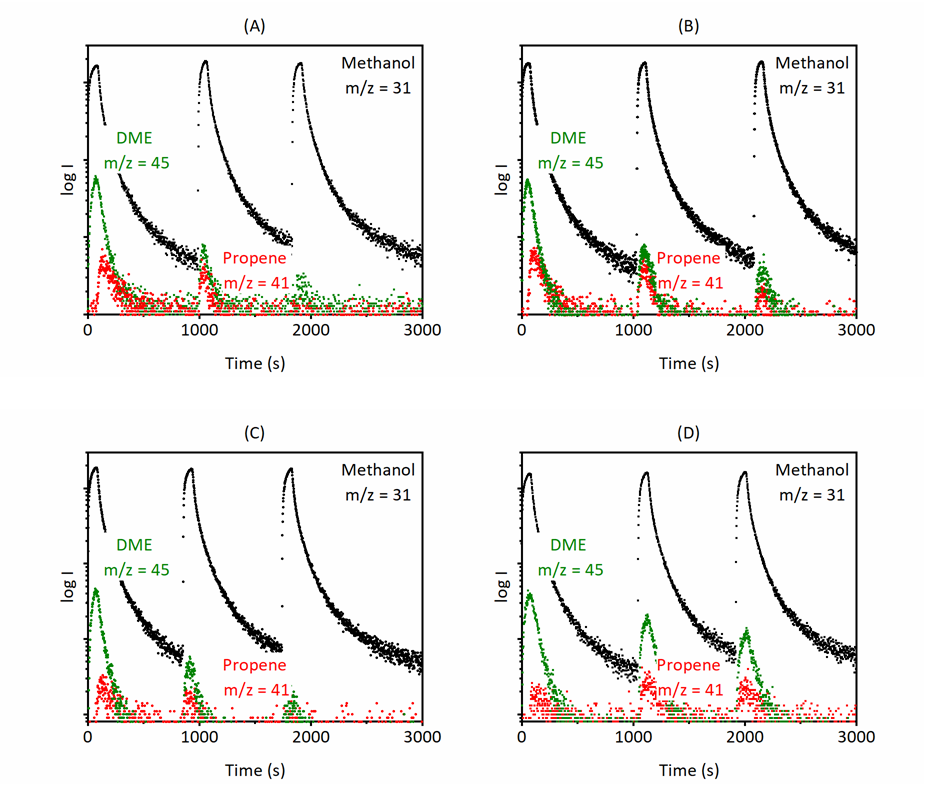

Figure S25. On-line MS analysis of gas phase products from Linkam FTIR cell recorded following three 8 µL pulses of CH_3OH at 623 K over samples: (A) LC-SAPO-34-A, (B) LC-SAPO-34-A-973-20, (C) LC-SAPO-34-B and (D) LC-SAPO-34-B-973-44. MS traces for this experiment were obtained on the Hiden instrument, measuring methanol (m/z = 31), DME (m/z = 45) and propene (m/z = 41).

S3. Summary scheme

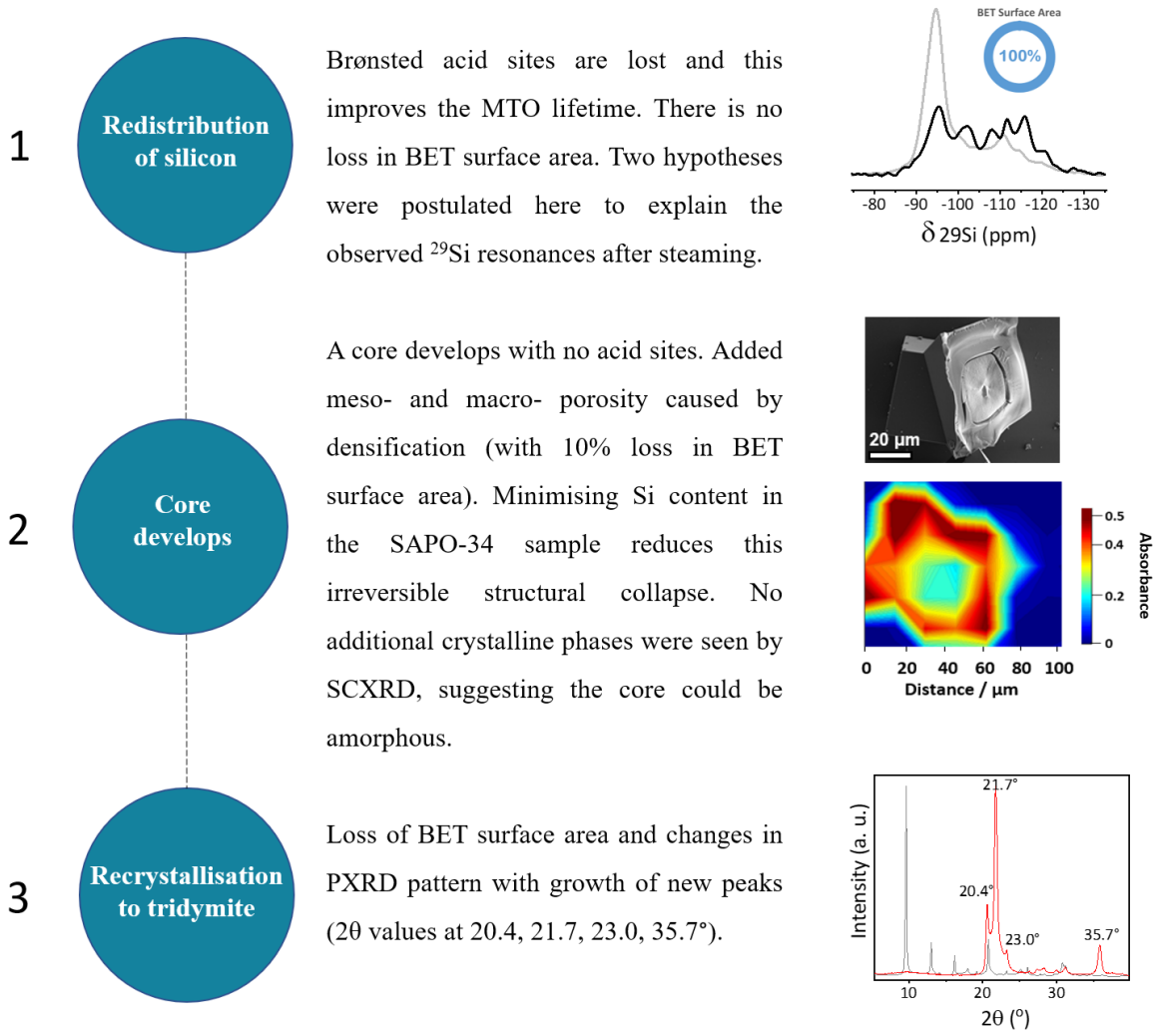

Figure S26. Three-stage transformation of SAPO-34 exposed to prolonged hydrothermal steaming as derived from this work.

References

[1] B. Arstad, A. Lind, J.H. Cavka, K. Thorshaug, D. Akporiaye, D. Wragg, H. Fjellvåg, A. Grønvold, T. Fuglerud, Structural Changes in SAPO-34 Due to Hydrothermal Treatment. A NMR, XRD, and DRIFTS Study, Micropor. Mesopor. Mat. 225 (2016) 421–431.